Chemical Physics Letters 824 (2023) 140551

Contents lists available at ScienceDirect

Chemical Physics Letters

journal homepage: www.elsevier.com/locate/cplett

Research paper

Synthesis of $NiCo_2O_4$ microflowers by facile hydrothermal method: Effect of precursor concentration

O.C. Pore [a], A.V. Fulari [b], C.D. Chavare [c], D.S. Sawant [d], S.S. Patil [e], R.V. Shejwal [a], V.J. Fulari [e], G.M. Lohar [a,*]

[a] Department of Physics, Lal Bahadur Shastri College of Arts, Science and Commerce, Satara 415002, India
[b] Division of Physics and Semiconductor Science, Dongguk University, Seoul 04620, South Korea
[c] Department of Physics, Annasaheb Magar Mahavidyalaya, Hadapsar (Pune), MH 411028, India
[d] Department of Physics, The Institute of Science, Dr. Homi Bhabha State University, Madam Cama Road, Mumbai 400032, India
[e] Department of Physics, Holography and Materials Research Laboratory, Shivaji University, Kolhapur, MH 416004, India

ARTICLE INFO

Keywords:
Hydrothermal
Supercapacitor
$NiCo_2O_4$
Microflowers

ABSTRACT

In this work, $NiCo_2O_4$ microflowers are developed via hydrothermal method. The impact of precursor concentration on morphology and supercapacitor performance is investigated. The XRD, FTIR and XPS study reveals the formation of $NiCo_2O_4$. The FE-SEM study shows the formation of microflower-like morphology. The $NiCo_2O_4$ with molar ratio Ni:Co = 1:2 exhibited a BET specific surface area of 147.3 $m^2\ g^{-1}$. The supercapacitor study confirms the optimized $NiCo_2O_4$ electrode showed a maximum sp. capacitance of 747.4 F g^{-1} at 5 mV s^{-1}. It exhibited highest energy density of 9.27 Wh kg^{-1} (@55.55 W kg^{-1}) and 82.32% capacity retention over 5000 cycles.

1. Introduction

In the last decades, research is more focused on modern electrode materials for energy storage devices (ESD) so as to complete the increasing demand for highly efficient renewable devices [1]. Among the various ESDs, supercapacitors are noteworthy candidates because of its excellent coulombic efficiency, high cyclic stability and higher power density than other ESDs [2]. The different conducting polymers [3], transition metal oxides like RuO_2 [4], MnO_2 [5], NiO [6], and Co_3O_4 [7], CeO_2 [8] has been widely studied as an electrode for pseudocapacitors. The ternary metal oxides (TMOs) deliver greater specific capacitance (sp. capacitance) than conducting polymers as it contains multi-electron redox reactions [9]. In addition, due to their rich redox-active sites and improved electronic conductivity, TMOs show better capacitive performance than single metal oxides [10]. Among the various TMOs, battery type nickel cobaltite ($NiCo_2O_4$) has been considered as promising electrode material in supercapacitor applications [11]. The high electrical conductivity and improved sp. capacitance of $NiCo_2O_4$ are due to the contributions from different valence states of the cobalt and nickel ions [12].

Researchers have tried to improve supercapacitor performance by synthesizing $NiCo_2O_4$ with different morphologies. Sethi et al. [13] developed $NiCo_2O_4$ nanorods using the low-temperature solvothermal method. The prepared $NiCo_2O_4$ nanorod reported 440 F g^{-1} sp. capacitance at a scan rate of 5 mV s^{-1}. Also, it exhibited 94% initial capacity retention over 2000 cycles. Waghmode et al. [14] prepared rodlike to flowerlike $NiCo_2O_4$ via chemical bath deposition method by varying reaction times. The optimized $NiCo_2O_4$ electrode achieved a maximum sp. capacitance of 540 F g^{-1} at a scan rate of 5 mV s^{-1} and 93.5% initial capacity retention over 1000 cycles. Han et al. [15] synthesized $NiCo_2O_4$ featherlike arrays by hydrothermal method. The $NiCo_2O_4$ electrode reported a maximum sp. capacitance of 450 F g^{-1} at 0.5 A g^{-1}. This electrode exhibited outstanding cyclic stability of 139.6% over 3000 cycles.

A literature survey showed that hydrothermal is a noteworthy technique for synthesizing different inorganic nanostructures with high complexity and structural specialties [10]. In the present investigation, we have synthesized a microflower-like structure of $NiCo_2O_4$ by using a hydrothermal method and used it as electrode material for supercapacitor application. The effect of Ni:Co concentration on the surface morphology and electrochemical supercapacitor performance of the $NiCo_2O_4$ material is investigated.

* Corresponding author.
E-mail address: gauravlohar24@gmail.com (G.M. Lohar).

https://doi.org/10.1016/j.cplett.2023.140551
Received 10 November 2022; Received in revised form 25 April 2023; Accepted 26 April 2023
Available online 29 April 2023

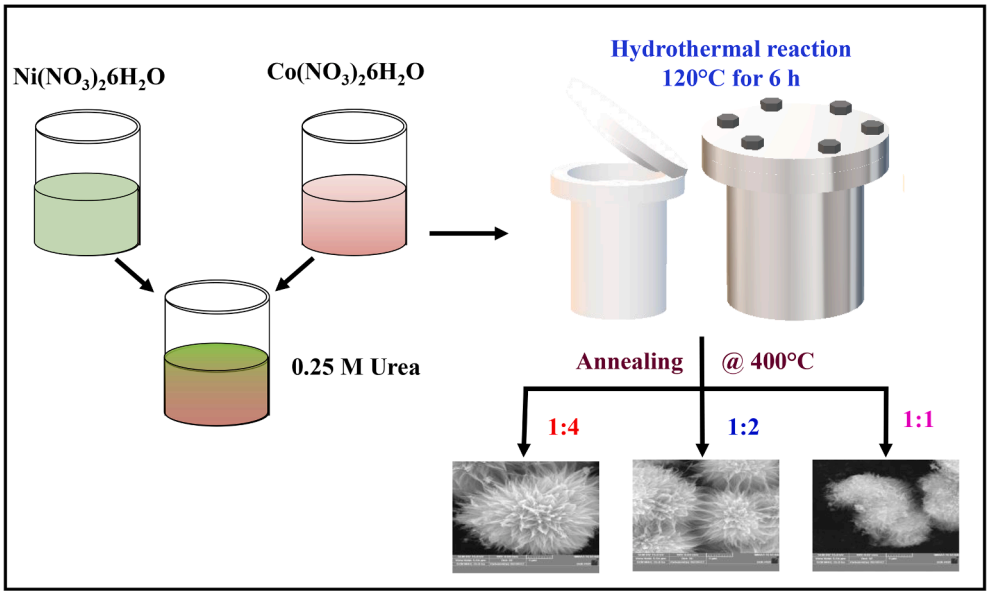

Fig. 1. Schematic presentation of hydrothermal synthesis of $NiCo_2O_4$ at different Ni:Co molar ratios.

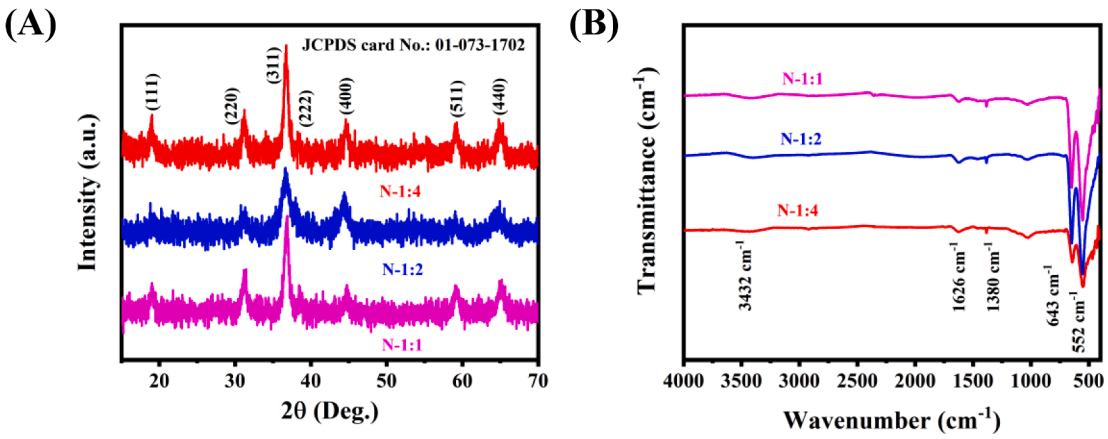

Fig. 2. (A) XRD patterns of $NiCo_2O_4$ samples synthesized by varying Ni:Co molar ratios. (B) FTIR patterns of different $NiCo_2O_4$ samples synthesized by varying Ni:Co molar ratios.

2. Experimental details

2.1. Synthesis of $NiCo_2O_4$ by varying Ni:Co molar ratios

The $NiCo_2O_4$ powders by varying Ni:Co molar ratios were prepared via facile hydrothermal route followed by annealing treatment. In the actual reaction process, 0.03 M $Ni(NO_3)_2 \cdot 6H_2O$, 0.12 M $Co(NO_3)_2 \cdot 6H_2O$, and 0.5 M of urea were dissolved in double distilled water (DDW) and stirred for 0.5 h. Then the whole solution was moved into a 100 mL Teflon-lined stainless-steel autoclave, and the reaction was carried out at 393 K for 6 h. After completion of reaction time, reaction products were washed with DDW and ethanol several times and dried at 333 K in a hot air oven overnight. Finally, the prepared powder was annealed at 673 K for 2 h. The obtained powder was named as N-1:4. Similarly, powders with different Ni:Co molar ratios were synthesized by taking molar ratios 1:2 and 1:1. Based on the molar ratios of Ni:Co precursors viz 1:4, 1:2, and 1:1 the obtained powders were named as N-1:4, N-1:2 and N-1:1 respectively. Fig. 1 shows the schematic diagram of the hydrothermal synthesis of $NiCo_2O_4$ at different Ni:Co molar ratios.

2.2. Reaction mechanism

The formation of $NiCo_2O_4$ by using urea ligand is explained as follows [16,17],

$$CO(NH_2)_2 + H_2O \rightarrow 2NH_3 + CO_2 \quad (1)$$

$$CO_2 + H_2O \rightarrow H_2CO_3 \rightarrow CO_3^{2-} + 2H^+ \quad (2)$$

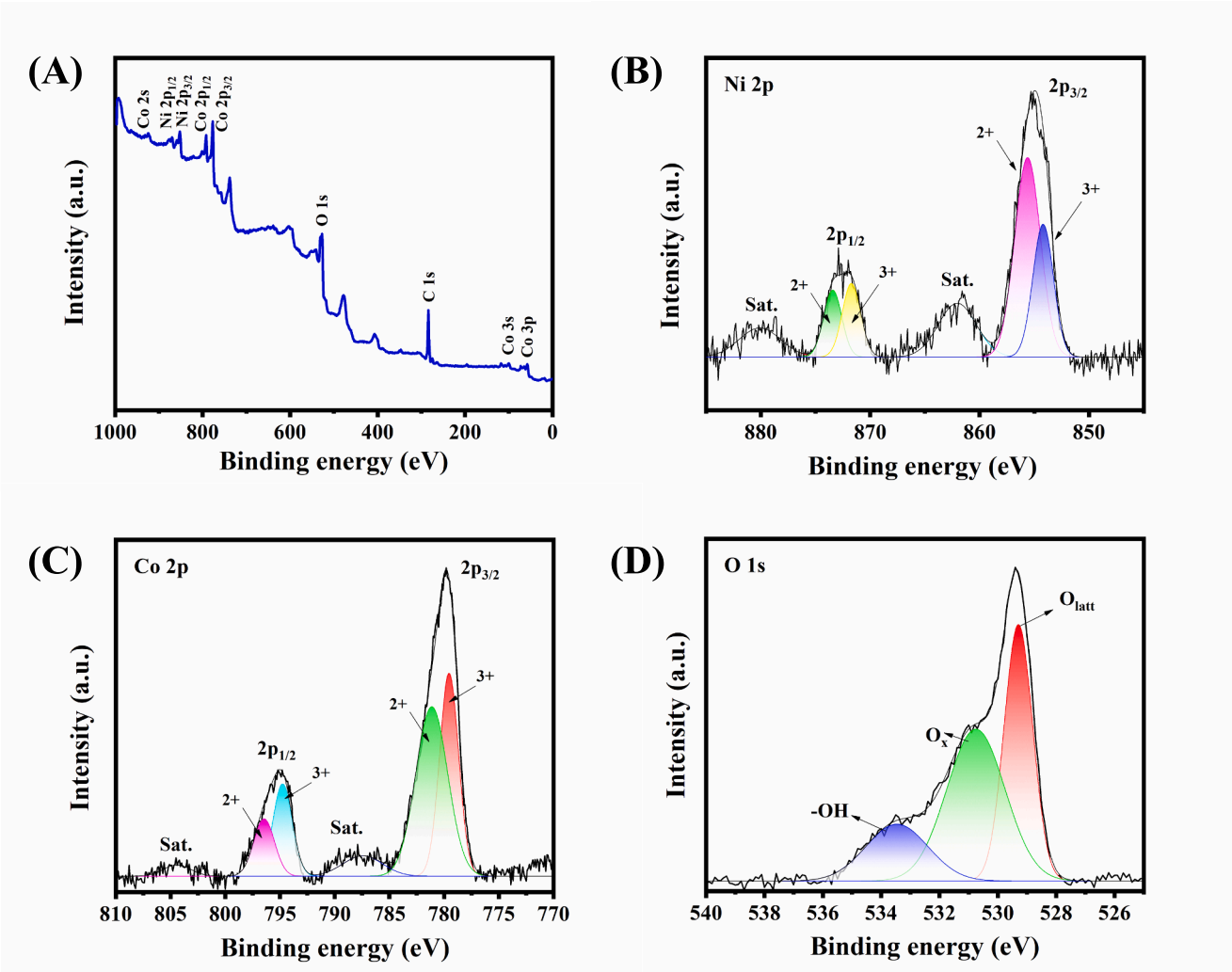

Fig. 3. XPS study of N-1:2 sample (A) Survey spectrum (B) Ni 2p (C) Co 2p (D) O 1s.

$$NH_3 + H_2O \rightarrow NH_3 \cdot H_2O \rightarrow NH_4^+ + OH^- \quad (3)$$

$$Ni^{2+} + 2Co^{2+} + 3xOH^- + 1.5(2-x)CO_3^{2-} + nH_2O \rightarrow NiCo_2(OH)_{3x}(CO_3)_{1.5(2-x)} \cdot nH_2O \quad (4)$$

$$2NiCo_2(OH)_{3x}(CO_3)_{1.5(2-x)} \cdot nH_2O + O_2 \rightarrow 2NiCo_2O_4 + 3(2-x)CO_2 + (3x+2n)H_2O \quad (5)$$

During the hydrothermal reaction, the Ni^{2+} and Co^{2+} metal cations react with CO_3^{2-} and OH^- anions that were released from the hydrolysis of urea. This reaction results in the nickel carbonate hydroxide hydrate and cobalt basic carbonate co-coprecipitate. This co-precipitate on annealing at 673 K in the presence of air for 2 h results in the formation of $NiCo_2O_4$ [18].

2.3. Preparation of working electrode

In order to prepare working electrode, the slurry was obtained by mixing $NiCo_2O_4$ powders as an active material, carbon black, and binder polyvinylidene fluoride (PVDF) in a mass ratio 80:10:10 in N-Methylpyrrolidone (NMP) as a solvent. The prepared slurry was coated on nickel foam (NF) (1 cm × 1 cm). The slurry coated NF was left to dry overnight at 80 °C. The resulting electrodes based on molar ratios of Ni: Co as 1:4, 1:2 and 1:1 was named Ns-1:4, Ns-1:2 and Ns-1:1, respectively and used for the electrochemical supercapacitor study.

3. Results and discussion

3.1. X-Ray diffraction (XRD) study

Fig. 2 (A) shows the XRD patterns of different $NiCo_2O_4$ nanostructures. The observed d-spacing values are well matched with JCPDS card number 01-073-1702. The peaks are noticed at an angle 18.94°, 31.16°, 36.79°, 38.40°, 44.68°, 59.19°, and 64.98° are assigned to the crystal planes (111), (220), (311), (222), (400), (511), and (440). It exhibited a cubic crystal structure with space group Fd-3m. No any

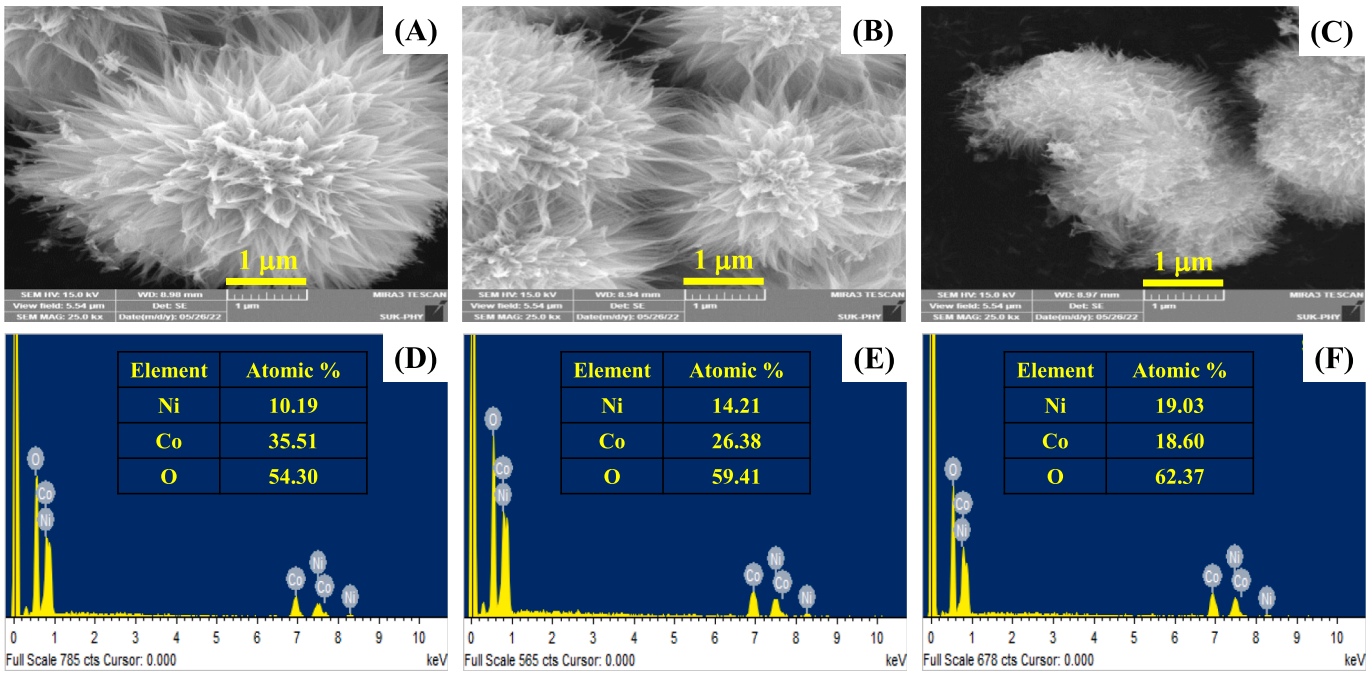

Fig. 4. FE-SEM images of $NiCo_2O_4$ samples synthesized by varying Ni:Co molar ratios (A) N-1:4, (B) N-1:2, and (C) N-1:1 and EDAX spectra of $NiCo_2O_4$ samples synthesized with different Ni:Co molar ratios (D) N-1:4, (E) N-1:2, and (F) N-1:1 respectively.

characteristic impurity peak was observed, which indicates the formation of high purity of $NiCo_2O_4$. The crystallite size is calculated for the plane (3 1 1) by using Scherrer's formula [19]. The obtained crystallite size values for N-1:4, N-1:2, and N-1:1 electrode is 15.19, 12.53, and 14.53 nm, respectively. The N-1:2 sample showed lowest crystallite size than the other samples.

3.2. Fourier transform infrared spectroscopic (FTIR) study

Further FTIR study of prepared $NiCo_2O_4$ powders was done to investigate the structural molecular changes and the formation of $NiCo_2O_4$ after annealing. Fig. 2 (B) shows the FTIR spectra of as-prepared different $NiCo_2O_4$ powders. In FTIR spectra the two sharp characteristic peaks at about 552 cm^{-1} and 643 cm^{-1} are related to the stretching vibrations of Ni–O and Co–O bonds, which confirms the formation of $NiCo_2O_4$ [20,21]. The relatively weak peaks at about 1626 cm^{-1} and 3432 cm^{-1} are originated from the O–H bending and stretching mode of vibration of absorbed water molecules [22]. The peak at 1380 cm^{-1} is related to the NO^{3-} anions [23]. The overall FTIR study confirms the formation of $NiCo_2O_4$. The peak at about 1100 cm^{-1} is corresponding to the C–O bending vibrations [24]. The peak at about 2330 cm^{-1} is related to the CO_2 vibrant may be due to the environmental factor [25].

3.3. X-ray photoelectron spectroscopy (XPS) study

The oxidation states and elementary compositions of the N-1:2 sample were analyzed by XPS study. The survey spectrum in Fig. 3 (A) indicates the presence of Ni, Co, O, and C elements, and no other obvious peaks are observed. The peak at about 284.3 eV is corresponding to the presence of environmental carbon [26]. In the high-resolution Ni 2p spectrum (Fig. 3 (B)) two shakeup satellites and two spin–orbit doublets (Ni^{2+} and Ni^{3+}) are present. The peaks at binding energy 854.2 eV and 871.7 eV are related to Ni^{2+} while the peaks at 855.6 eV and 873.5 eV are attributed to Ni^{3+}. Similarly, the Co 2p spectrum (Fig. 3 (C)) can be fitted into two shakeup satellites and two spin–orbit doublets (Co^{2+} and Co^{3+}). The peaks at binding energy 781.2 eV and 796.5 eV are related to Co^{2+} while the peaks at 780.1 eV and 794.7 eV are attributed to Co^{3+}. In the O 1s spectrum (Fig. 3 (D)) the peak at about 529.3 eV and 531.1 eV can be assigned to the lattice oxygen from the porous $NiCo_2O_4$ and

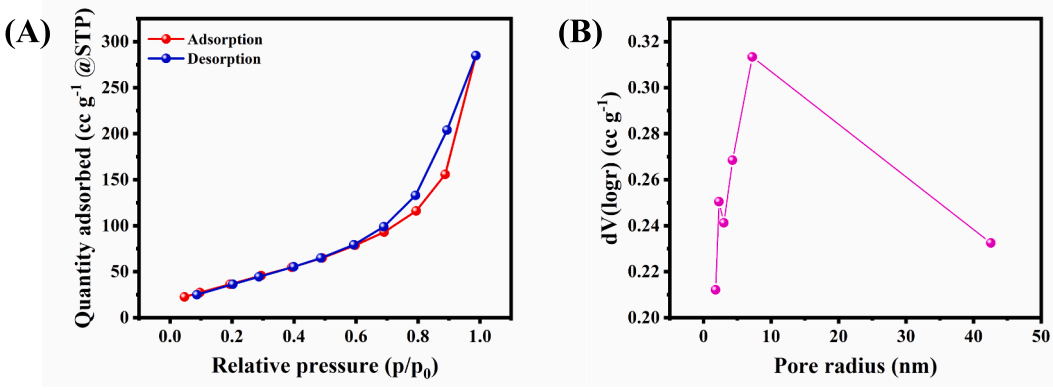

Fig. 5. (A) Nitrogen adsorption and desorption isotherms measured at 77 K and (B) BJH pore size distribution of N-1:2 sample.

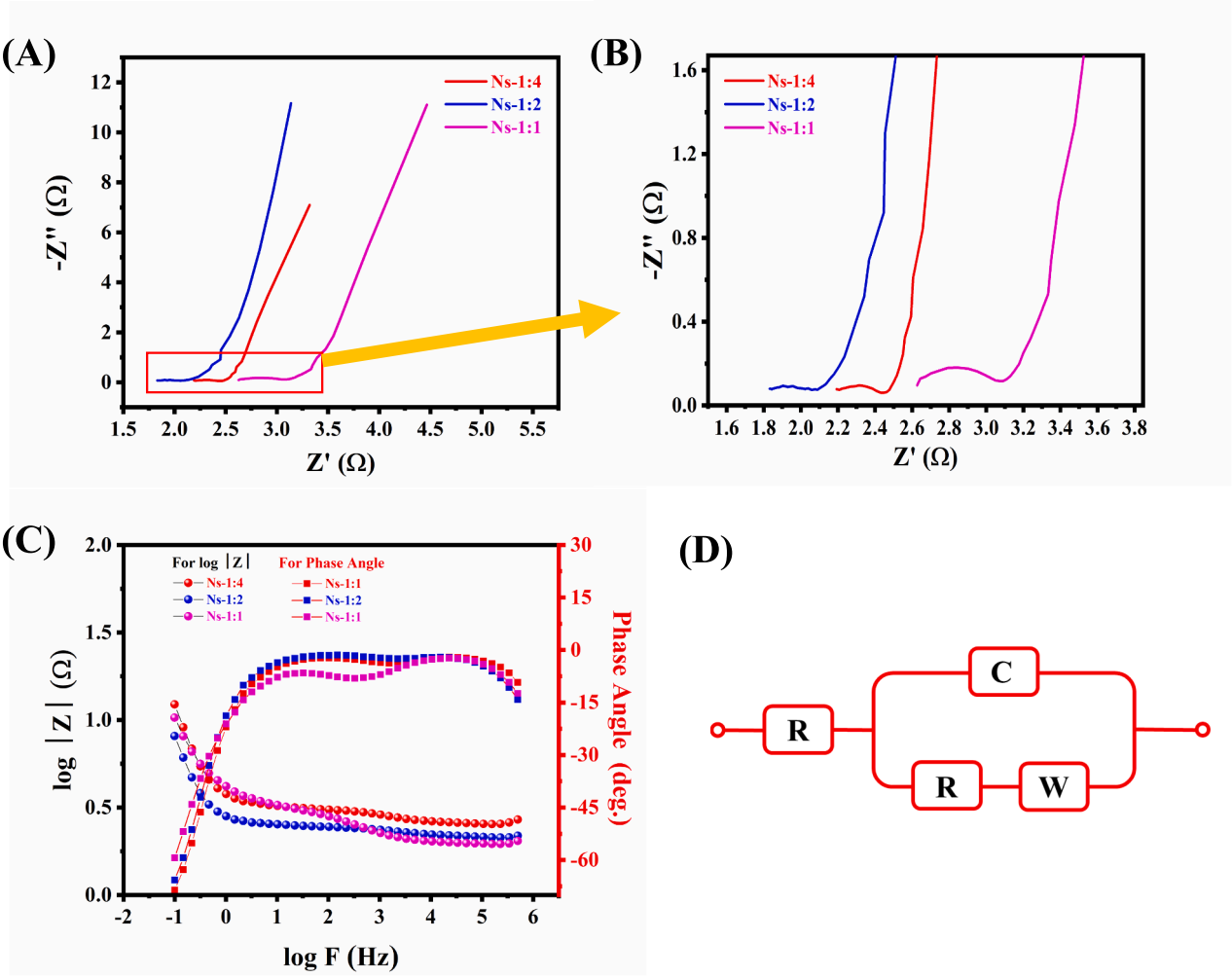

Fig. 6. EIS study of $NiCo_2O_4$ samples synthesized by varying Ni:Co molar ratios (A) Nyquist plot (B) Enlarged view of Nyquist plot, (C) Bode plot, (D) Equivalent circuit diagram.

$O_x^-(O^-$ or $O_2^-)$ ions absorbed by oxygen-deficient region of $NiCo_2O_4$ respectively. The peak at about 533.1 eV is due to oxygen ions in low coordination on the surface with defect sites [26].

3.4. Field emission scanning electron microscopic (FE-SEM) study

Fig. 4 (A-C) depicts the FE-SEM images of N-1:4, N-1:2, and N-1:1 samples synthesized by changing Ni:Co molar ratios. The FESEM study shows the formation of microflowers. Initially, when the Ni:Co molar ratio was 1:4, the microflowers with a diameter of about 5 μm are observed (Fig. 4 (A)). The petals of this microflower are made up of spikes-like rods. When Ni:Co molar ratio was 1:2, then the size of microflower was lowered, and it is about 2.5 μm (Fig. 4 (B)). The microflowers are hierarchically connected with each other, seems their spike rod-like petals are interconnected with each other to form a mesoporous structure. Such morphology is beneficial for better electrolyte penetration in the bulk of the material. As the molar ratio changes to 1:1, the petals of microflowers are disappeared, and cluster-like morphology is observed (Fig. 4 (C)). The formation of such diverse morphologies at different precursor concentrations depends on intrinsic crystal contraction, Vander Waals forces, Ostwald ripening, hydrogen bonding, crystal field attraction, hydrophobic attraction, and electrostatic and dipolar fields [27]. The EDAX spectrum of N-1:4, N-1:2, and N-1:1 samples are shown in Fig. 4 (D-F). The atomic percentage of Ni, Co, and O elements is provided in the inset of EDAX spectra of each N-1:4, N-1:2, and N-1:1 sample. The EDAX spectra show signals corresponding to the presence of Ni, Co, and O species on its surface. The EDAX data confirmed the formation of the $NiCo_2O_4$ phase in the sample.

3.5. Brunauer–Emmett–Teller (BET) study

For the BET analysis, N-1:2 powder sample was used. Fig. 5 (A) represents the N_2 adsorption–desorption isotherm while Fig. 5 (B) represents their corresponding BJH pore size distribution curve. According to the IUPAC classification, as shown in Fig. 5 (B) the isotherm exhibited H3 hysteresis and type IV isotherm [28]. This type IV isotherm possesses a small hysteresis loop observed at relative pressure 0.6–1.0. The Ni-1:2 sample with microflower-like morphology exhibited BET specific surface area of 147.3 $m^2\ g^{-1}$. From BJH analysis the values of average pore size and total pore volume obtained are 1.78 nm and 0.44 cc g^{-1} respectively. Such mesoporous microflowers with high surface area, large pore volume as well as small pore size are beneficial for fast electron transfer and help to enhance electrochemical performance [29].

3.6. Electrochemical impedance spectroscopic (EIS) study

The EIS study was performed in order to investigate the electrochemical behavior of electrodes at the electrode–electrolyte interface [30–32]. The Nyquist plots of Ns-1:4, Ns-1:2, and Ns-1:1 electrode is given in Fig. 6 (A). Fig. 6 (B) presents the enlarged view of the Nyquist plot. The R_s values obtained from Nyquist plot for Ns-1:4, Ns-1:2, and

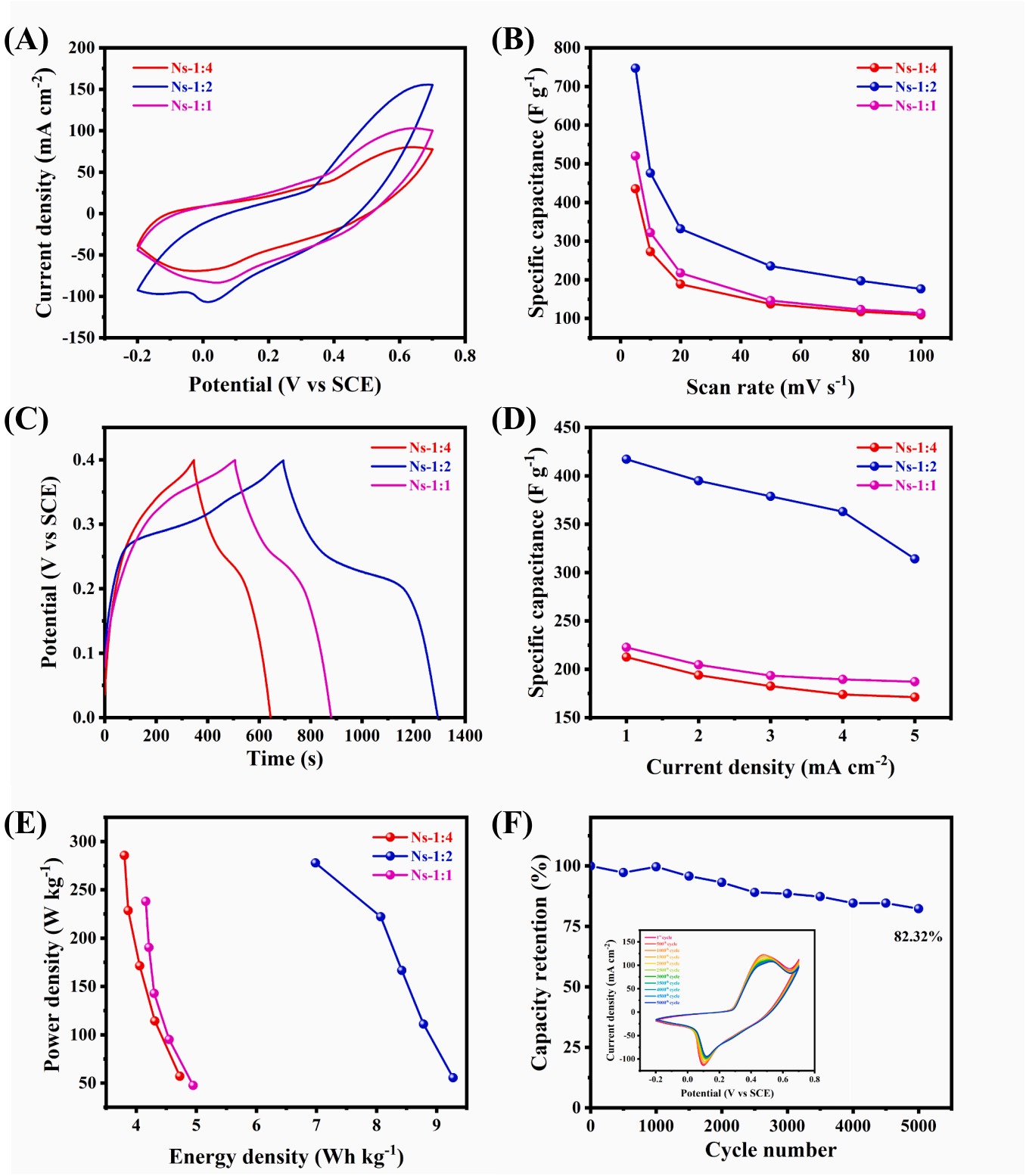

Fig. 7. Electrochemical supercapacitor study of $NiCo_2O_4$ samples synthesized by varying Ni:Co molar ratios (A) Comparative CV curves of all electrodes at scan rate of 100 mV s^{-1}, (B) Sp. capacitance as a function of scan rate of all $NiCo_2O_4$ samples, (C) Comparative GCD curves of all electrodes at 1 mA cm^{-2} current density (D) Sp. capacitance as a function of the current density of all $NiCo_2O_4$ samples, (E) Regone plot of Ns-1:4, Ns-1:2, and Ns-1:1 electrode (F) Cyclic stability of Ns-1:2 electrode (Inset: Various CV cycles of cyclic stability at different cycle numbers of Ns-1:2 electrode).

Ns-1:1 electrodes are 2.18, 1.84, and 2.60 Ω cm^{-2} respectively. The R_{ct} values for Ns-1:4, Ns-1:2, and Ns-1:1 electrodes are 0.41, 0.35, and 0.49 Ω cm^{-2} respectively. The lower values of R_s and R_{ct} reveal good electrical conductivity and better attachment of active material with the current collector [33]. Fig. 6 (C) presents the Bode plot of Ns-1:4, Ns-1:2, and Ns-1:1 electrodes. Fig. 6 (D) shows the corresponding equivalent circuit diagram.

Table 1
Comparative electrochemical supercapacitor study of present work and previously reported literature.

Sr. No	Material	Method	Electrolyte	Sp. Capacitance (F g^{-1})	Stability	Ref.
	$NiCo_2O_4$	Solvothermal	2 M KOH	440 (5 mV s^{-1})	94% over 2000 cycles	[13]
	$MnO_2/NiCo_2O_4$	Hydrothermal	1 M KOH	634.37 (0.5 A g^{-1})	96.3% over 3000 cycles	[36]
	C@$NiCo_2O_4$	Hydrothermal	6 M KOH	404 (1 A g^{-1})	87.1% over 2000 cycles	[37]
	$NiCo_2O_4$	Hydrothermal	1 M KOH	438.7 (1 A g^{-1})	76.5% over 2000 cycles	[38]
	$NiCo_2O_4$	dealloying process	2 M KOH	663 (1 A g^{-1})	82.1% over 5000 cycles	[39]
	$NiCo_2O_4$/GA	Hydrothermal	6 M KOH	720 (1 A g^{-1})	84% over 1000 cycles	[40]
	$NiCo_2O_4$	Hydrothermal	2 M KOH	450 (0.5 A g^{-1})	139.6% over 3000 cycles	[15]
	$NiCo_2O_4$	Hydrothermal	1 M KOH	361 (5 A g^{-1})	105% over 2000 cycles	[41]
	$NiCo_2O_4$	Hydrothermal	2 M KOH	183.71 (1 A g^{-1})	Good stability over 3000 cycles	[42]
	$NiCo_2O_4$	Hydrothermal	2 M KOH	332 (5 mV s^{-1})	86% after 2000 cycles	[43]
	$NiCo_2O_4$	Hydrothermal	2 M KOH	294 (1 A g^{-1})	–	[27]
	$NiCo_2O_4$	Hydrothermal	1 M KOH	747.4 (5 mV s^{-1})	82.32% over 5000 cycles	**Present study**

3.7. Electrochemical supercapacitor study

The electrochemical supercapacitor properties of as-prepared (Ns-1:4, Ns-1:2, and Ns-1:1) electrodes were done by cyclic voltammetry (CV) and galvanostatic charge–discharge (GCD) study. The three-electrode system with platinum wire as a counter electrode, saturated calomel electrode (SCE) as a reference electrode, and fabricated $NiCo_2O_4$ electrodes as working electrodes. Here 1 M KOH was used as an electrolyte.

The comparison of CV curves of different NiCo2O4 electrodes at 100 mV s^{-1} scan rate are mentioned in Fig. 7 (A). Here, we can observe that the electrode Ns-1:2 showed a maximum area under the curve. The CV curves of different $NiCo_2O_4$ samples at various scan rates are presented in Fig. S1 (A-C). All CV curves show the redox peaks. The oxidation and reduction peaks observed in all samples may be ascribed to the faradaic redox reactions [34],

$$NiCo_2O_4 + H_2O + OH^- \leftrightarrow 2CoOOH + NiOOH + e^- \quad (6)$$

$$2CoOOH + OH^- \leftrightarrow CoO_2 + H_2O + e^- \quad (7)$$

The graph of estimated sp. capacitance values as a function of scan rate of all samples is mentioned in Fig. 7 (B). The utmost sp. capacitance values calculated from CV curves for Ns-1:4, Ns-1:2, and Ns-1:1 electrodes are 435.38, 747.40, and 520.31 F g^{-1} at 5 mV s^{-1} respectively. The comparative GCD curves of different $NiCo_2O_4$ electrodes at 1 mA cm^{-2} are mentioned in Fig. 7 (C). The galvanostatic charge–discharge curves of Ns-1:4, Ns-1:2, and Ns-1:1 electrode is displayed in Fig. S2 (A-C). The estimated sp. capacitance values as a function of the current density of all samples are mentioned in Fig. 7 (D). The maximum sp. capacitance values calculated from GCD curves for Ns-1:4, Ns-1:2, and Ns-1:1 electrodes are 267.2, 417.33, and 222.66 F g^{-1} at 1 mA cm^{-2}, respectively. The estimated values of energy density and power density are mentioned in Fig. 7 (E). The maximum energy density for Ns-1:2 electrode is 9.27 Wh kg^{-1}, and their corresponding power density is 55.55 W kg^{-1}. As Ns-1:2 electrode showed maximum sp. capacitance as compared to the Ns-1:4 and Ns-1:1 electrodes, the cyclic stability was taken for the Ns-1:2 electrode. Fig. 7 (F) shows the cyclic stability of the Ns-1:2 electrode. The inset of Fig. 7 (F) shows the CV cycles of cyclic stability. The Ns-1:2 electrode exhibited excellent cyclic stability of about 82.32% over 5000 cycles. The coulombic efficiency of Ns-1:4, Ns-1:2, and Ns-1:1 electrodes as a function of current density is provided in Fig. S3. The coulombic efficiency is low at lower current density and high at high current density. This is may be due to shorter charging-discharging time as well as lower charge loss at higher current densities [35]. The excellent supercapacitor performance and cyclic stability of Ns-1:2 electrode are attributed to the microflower-like morphology. The spike rod-like petals are interconnected with each other to form a mesoporous structure. Such structure is beneficial for the effective penetration of electrolyte ions in the bulk of the material and resulted in high electrochemical supercapacitor performance than other electrodes. The comparative supercapacitor performance of the present work and previously reported work is mentioned in Table 1.

4. Conclusion

In summary, the $NiCo_2O_4$ nanostructures by varying Ni:Co molar ratios have been synthesized by the hydrothermal method. The formation of $NiCo_2O_4$ is confirmed by the XRD study. It exhibited a cubic crystal structure with space group Fd-3m. The $NiCo_2O_4$ with Ni:Co molar ratio 1:2 exhibited the lowest crystallite size as compared to the other samples. Further formation of $NiCo_2O_4$ is confirmed by FTIR. The XPS study also confirms the formation of $NiCo_2O_4$. The FE-SEM micrographs confirm the formation of microflowers. The $NiCo_2O_4$ with molar ratio Ni:Co = 1:2 exhibited a BET specific surface area of 147.3 m^2 g^{-1}. The EIS analysis indicates the sample with Ni:Co molar ratio 1:2 showed the lowest R_s value as compared to the other electrodes. The electrochemical supercapacitor study showed $NiCo_2O_4$ with Ni:Co molar ratio 1:2 exhibited a maximum sp. capacitance of 747.4 F g^{-1} at 5 mV s^{-1} and capacity retention of 82.32% over 5000 CV cycles. Also, it showed the highest energy density of 9.27 Wh kg^{-1}, and its corresponding power density is 55.55 W kg^{-1}. The XRD, FE-SEM, and EIS results are consistent with supercapacitor results. The spike rod-like petals are interconnected with each other to form a mesoporous structure. Such structure is beneficial for the effective penetration of electrolyte ions in the bulk of the material and resulted in high supercapacitor performance as compared to other electrodes.

CRediT authorship contribution statement

O.C. Pore: Methodology, Visualization, Investigation, Writing – original draft. **A.V. Fulari:** Visualization, Investigation. **C.D. Chavare:** Formal analysis, Data curation. **D.S. Sawant:** Formal analysis. **S.S.**

Patil: Data curation. **R.V. Shejwal:** Supervision, Writing – review & editing. **V.J. Fulari:** Supervision, Writing – review & editing. **G.M. Lohar:** Conceptualization.

Declaration of Competing Interest

The authors declare that they have no known competing financial interests or personal relationships that could have appeared to influence the work reported in this paper.

Data availability

Data will be made available on request.

Acknowledgment

Dr. G. M. Lohar is thankful to DST-SERB, Government of India, for providing funds under the ECRA scheme File No: ECR/2017/002099.

Appendix A. Supplementary data

Supplementary data to this article can be found online at https://doi.org/10.1016/j.cplett.2023.140551.

References

[1] J.P. Perdew, J.A. Chevary, S.H. Vosko, K.A. Jackson, M.R. Pederson, D.J. Singh, C. Fiolhais, Atoms, molecules, solids, and surfaces: Applications of the generalized gradient approximation for exchange and correlation, Phys. Rev. B 46 (1992) 6671–6687, https://doi.org/10.1103/PhysRevB.46.6671.

[2] B.P. Relekar, S.A. Mahadik, S.T. Jadhav, A.S. Patil, R.R. Koli, G.M. Lohar, V. J. Fulari, Effect of Electrodeposition Potential on Surface Free Energy and Supercapacitance of MnO2 Thin Films, J. Electron. Mater. 47 (2018) 2731–2738, https://doi.org/10.1007/s11664-018-6109-9.

[3] B.P. Relekar, A.V. Fulari, G.M. Lohar, V.J. Fulari, Development of Porous Manganese Oxide/Polyaniline Composite Using Electrochemical Route for Electrochemical Supercapacitor, J. Electron. Mater. 48 (2019) 2449–2455, https://doi.org/10.1007/s11664-019-07039-3.

[4] R. Thangappan, M. Arivanandhan, R. Dhinesh Kumar, R. Jayavel, Facile synthesis of RuO2 nanoparticles anchored on graphene nanosheets for high performance composite electrode for supercapacitor applications, J. Phys. Chem. Solids 121 (2018) 339–349, https://doi.org/10.1016/j.jpcs.2018.05.049.

[5] B. Pandit, E.S. Goda, M.H. Abu Elella, A. ur Rehman, S. Eun Hong, S.R. Rondiya, P. Barkataki, S.F. Shaikh, A.M. Al-Enizi, S.M. El-Bahy, K. Ro Yoon, One-pot hydrothermal preparation of hierarchical manganese oxide nanorods for high-performance symmetric supercapacitors, J. Energy Chem. 65 (2022) 116–126.

[6] O.C. Pore, A.V. Fulari, N.B. Velha, V.G. Parale, H.H. Park, R.V. Shejwal, V.J. Fulari, G.M. Lohar, Hydrothermally synthesized urchinlike NiO nanostructures for supercapacitor and nonenzymatic glucose biosensing application, Mater. Sci. Semicond. Process. 134 (2021), 105980, https://doi.org/10.1016/j.mssp.2021.105980.

[7] O.C. Pore, A.V. Fulari, R.K. Kamble, A.S. Shelake, N.B. Velhal, V.J. Fulari, G. M. Lohar, Hydrothermally synthesized Co_3O_4 microflakes for supercapacitor and non-enzymatic glucose sensor, J. Mater. Sci.: Mater. Electron. 32 (15) (2021) 20742–20754.

[8] B. Pandit, N. Kumar, P.M. Koinkar, B.R. Sankapal, Solution processed nanostructured cerium oxide electrode: Electrochemical engineering towards solid-state symmetric supercapacitor device, J. Electroanal. Chem. 839 (2019) 96–107, https://doi.org/10.1016/J.JELECHEM.2019.02.047.

[9] X. Tian, J. Dai, L. Wang, A. Xie, J. He, Y. Yan, Vertically/parallelly orientated growth of $NiCo_2O_4$ nanosheet onto surface of hierarchically N-doped porous carbon for improved supercapacitor, Mater. Technol. 35 (2020) 463–474, https://doi.org/10.1080/10667857.2019.1699263.

[10] O.C. Pore, A.V. Fulari, R.V. Shejwal, V.J. Fulari, G.M. Lohar, Review on recent progress in hydrothermally synthesized MCo_2O_4/rGO composite for energy storage devices, Chem. Eng. J. 426 (2021), 131544, https://doi.org/10.1016/j.cej.2021.131544.

[11] C. Wang, G. Sui, D. Guo, J. Li, X. Ma, Y. Zhuang, D.F. Chai, Oxygen vacancies-rich $NiCo_2O_{4-4x}$ nanowires assembled on porous carbon derived from cigarette ash: A competitive candidate for hydrogen evolution reaction and supercapacitor, J. Energy Storage. 50 (2022), 104280, https://doi.org/10.1016/j.est.2022.104280.

[12] C. Wang, G. Sui, D. Guo, J. Li, Y. Zhuang, W. Guo, Y. Zhou, X. Yang, D.F. Chai, Inverted design of oxygen vacancies modulated $NiCo_2O_4$ and Co_3O_4 microspheres with superior specific surface area as competitive bifunctional materials for supercapacitor and hydrogen evolution reaction, J. Energy Storage. 49 (2022), 104083, https://doi.org/10.1016/J.EST.2022.104083.

[13] M. Sethi, D.K. Bhat, Facile solvothermal synthesis and high supercapacitor performance of $NiCo_2O_4$ nanorods, J. Alloys Compd. 781 (2019) 1013–1020, https://doi.org/10.1016/J.JALLCOM.2018.12.143.

[14] R.B. Waghmode, A.P. Torane, Role of deposition time on synthesis of high-performance $NiCo_2O_4$ supercapacitors, J. Mater. Sci. Mater. Electron. 28 (2017) 9575–9583, https://doi.org/10.1007/s10854-017-6705-0.

[15] D. Han, J. Wei, S. Wang, Y. Pan, J. Xue, Y. Wei, Feather-like $NiCo_2O_4$ self-assemble from porous nanowires as binder-free electrodes for low charge transfer resistance, Front. Mater. Sci. 14 (4) (2020) 450–458.

[16] Y. Zhang, J. Wang, J. Ye, P. Wan, H. Wei, S. Zhao, T. Li, S. Hussain, $NiCo_2O_4$ arrays nanostructures on nickel foam: Morphology control and application for pseudocapacitors, Ceram. Int. 42 (2016) 14976–14983, https://doi.org/10.1016/j.ceramint.2016.06.142.

[17] T. Wang, H. Zhang, H. Luo, M. He, W. Wang, Y. Dai, Controlled synthesis of $NiCo_2O_4$ nanowires and nanosheets on reduced graphene oxide nanosheets for supercapacitors, J. Solid State Electrochem. 19 (2015) 3309–3317, https://doi.org/10.1007/s10008-015-2940-6.

[18] E.R. Ezeigwe, P.S. Khiew, C.W. Siong, M.T.T. Tan, Solvothermal synthesis of $NiCo_2O_4$ nanocomposites on liquid-phase exfoliated graphene as an electrode material for electrochemical capacitors, J. Alloys Compd. 693 (2017) 1133–1142, https://doi.org/10.1016/J.JALLCOM.2016.09.244.

[19] G.M. Lohar, S.T. Jadhav, M.V. Takale, R.A. Patil, Y.R. Ma, M.C. Rath, V.J. Fulari, Photoelectrochemical cell studies of Fe^{2+} doped ZnSe nanorods using the potentiostatic mode of electrodeposition, J. Colloid Interface Sci. 458 (2015) 136–146, https://doi.org/10.1016/j.jcis.2015.07.046.

[20] S.A. Makhlouf, Z.H. Bakr, K.I. Aly, M.S. Moustafa, Structural, electrical and optical properties of Co_3O_4 nanoparticles, Superlattices Microstruct. 64 (2013) 107–117, https://doi.org/10.1016/j.spmi.2013.09.023.

[21] D.D.M. Prabaharan, K. Sadaiyandi, M. Mahendran, S. Sagadevan, Precipitation method and characterization of cobalt oxide nanoparticles, Appl. Phys. A Mater. Sci. Process. 123 (2017) 264, https://doi.org/10.1007/s00339-017-0786-8.

[22] G. Xu, Z. Zhang, X. Qi, X. Ren, S. Liu, Q. Chen, Z. Huang, J. Zhong, Hydrothermally synthesized $FeCo_2O_4$ nanostructures: Structural manipulation for high-performance all solid-state supercapacitors, Ceram. Int. 44 (2018) 120–127, https://doi.org/10.1016/j.ceramint.2017.09.146.

[23] V. Venkatachalam, A. Alsalme, A. Alghamdi, R. Jayavel, Hexagonal-like $NiCo_2O_4$ nanostructure based high-performance supercapacitor electrodes, Ionics 23 (4) (2017) 977–984.

[24] S.S. Pradeepa, P. Rajkumar, K. Diwakar, K. Sutharthani, R. Subadevi, M. Sivakumar, A Facile One-Pot Hydrothermal Synthesis of Zn, Mn Co-Doped $NiCo_2O_4$ as an Efficient Electrode for Supercapacitor Applications, ChemistrySelect 6 (2021) 6851–6862, https://doi.org/10.1002/SLCT.202101708.

[25] M. Silambarasan, P.S. Ramesh, D. Geetha, Facile one-step synthesis, structural, optical and electrochemical properties of $NiCo_2O_4$ nanostructures, J. Mater. Sci. Mater. Electron. 28 (2017) 323–336, https://doi.org/10.1007/S10854-016-5527-9/METRICS.

[26] S.B. Dhavale, V.L. Patil, S.A. Beknalkar, A.M. Teli, A.H.A.P. Patil, A.H.A.P. Patil, J. C. Shin, P.S. Patil, Study of solvent variation on controlled synthesis of different nanostructured $NiCo_2O_4$ thin films for supercapacitive application, J. Colloid Interface Sci. 588 (2021) 589–601, https://doi.org/10.1016/j.jcis.2020.12.057.

[27] B. Saravanakumar, T. Priyadharshini, G. Ravi, V. Ganesh, A. Sakunthala, R. Yuvakkumar, Hydrothermal synthesis of spherical $NiCo_2O_4$ nanoparticles as a positive electrode for pseudocapacitor applications, J. Sol-Gel Sci. Technol. 84 (2017) 297–305, https://doi.org/10.1007/s10971-017-4504-y.

[28] Z.A. Alothman, A Review: Fundamental Aspects of Silicate Mesoporous Materials, Mater 5 (2012) 2874–2902. doi: 10.3390/MA5122874.

[29] K. Xu, J. Yang, S. Li, Q. Liu, J. Hu, Facile synthesis of hierarchical mesoporous $NiCo_2O_4$ nanoflowers with large specific surface area for high-performance supercapacitors, Mater. Lett. 187 (2017) 129–132, https://doi.org/10.1016/J.MATLET.2016.10.083.

[30] B. Pandit, S.A. Pande, B.R. Sankapal, Facile SILAR Processed Bi2S3:PbS Solid Solution on MWCNTs for High-performance Electrochemical Supercapacitor, Chin. J. Chem. 37 (2019) 1279–1286, https://doi.org/10.1002/CJOC.201900222.

[31] E.S. Goda, B. Pandit, S.E. Hong, B.S. Singu, S.K. Kim, E.B. Moustafa, K.R. Yoon, Zeolitic imidazolate framework-67 derived Al-Co-S hierarchical sheets bridged by nitrogen-doped graphene: Incorporation of PANI derived carbon nanorods for solid-state asymmetric supercapacitors, J. Energy Chem. 74 (2022) 429–445, https://doi.org/10.1016/J.JECHEM.2022.07.033.

[32] B. Pandit, B.R. Sankapal, Cerium Selenide Nanopebble/Multiwalled Carbon Nanotube Composite Electrodes for Solid-State Symmetric Supercapacitors, ACS Appl. Nano Mater. 5 (2022) 3007–3017, https://doi.org/10.1021/acsanm.2c00374.

[33] P. Liu, M. Yang, S. Zhou, Y. Huang, Y. Zhu, Hierarchical shell-core structures of concave spherical NiO nanospines@carbon for high performance supercapacitor electrodes, Electrochim. Acta 294 (2019) 383–390, https://doi.org/10.1016/j.electacta.2018.10.112.

[34] A.K. Yedluri, H.J. Kim, Enhanced electrochemical performance of nanoplate nickel cobaltite ($NiCo_2O_4$) supercapacitor applications, RSC Adv. 9 (2019) 1115–1122, https://doi.org/10.1039/C8RA09081E.

[35] K. Wang, X. Wang, D. Zhang, H. Wang, Z. Wang, M. Zhao, R. Xi, H. Wu, M. Zheng, Interpenetrated nano-MOFs for ultrahigh-performance supercapacitors and excellent dye adsorption performance, CrystEngComm 20 (2018) 6940–6949, https://doi.org/10.1039/C8CE01067F.

[36] N.a. Zhang, C. Xu, H. Wang, J. Zhang, Y. Liu, Y. Fang, Assembly of the hierarchical MnO2@$NiCo_2O_4$ core–shell nanoflower for supercapacitor electrodes, J. Mater. Sci.: Mater. Electron. 32 (2) (2021) 1787–1799.

[37] W. Li, F. Yang, Z. Hu, Y. Liu, Template synthesis of C@$NiCo_2O_4$ hollow microsphere as electrode material for supercapacitor, J. Alloys Compd. 749 (2018) 305–312, https://doi.org/10.1016/j.jallcom.2018.03.046.

[38] B. Li, Q. Sun, R. Yang, D. Li, Z. Li, Simple preparation of graphene-decorated $NiCo_2O_4$ hollow nanospheres with enhanced performance for supercapacitor, J. Mater. Sci.: Mater. Electron. 29 (9) (2018) 7681–7691.

[39] Q. Zhou, S. Jiao, B. Zheng, Z. Li, Preparation and Pseudo-capacitance Performance of $NiCo_2O_4$ Nanosheets, Chem. Res. Chinese Univ. 35 (2019) 957–961, https://doi.org/10.1007/s40242-019-9172-8.

[40] H. Jiu, L. Jiang, Y. Gao, Q. Zhang, L. Zhang, Synthesis of three-dimensional graphene aerogel-supported $NiCo_2O_4$ nanowires for supercapacitor application, Ionics 25 (9) (2019) 4325–4331.

[41] S. Yadav, A. Sharma Ghrera, A. Devi, Hierarchical grass-like $NiCo_2O_4$ nanowires grown on nickel foam as a binder-free supercapacitor electrode, Mater. Today: Proc. 74 (2023) 281–288.

[42] J. Qin, Temperature-induced Hollow Hierarchical $NiCo_2O_4$ Microspheres for High Performance Pseudocapacitors, Int. J. Electrochem. Sci. 17 (2022) ArticleID: 220335. doi: 10.20964/2022.03.17.

[43] T. Kim, A. Ramadoss, B. Saravanakumar, G.K. Veerasubramani, S.J. Kim, Synthesis and characterization of $NiCo_2O_4$ nanoplates as efficient electrode materials for electrochemical supercapacitors, Appl. Surf. Sci. 370 (2016) 452–458, https://doi.org/10.1016/j.apsusc.2016.02.147.